Tréhu, A.M., Bohrmann, G., Torres, M.E., and Colwell, F.S. (Eds.)
Proceedings of the Ocean Drilling Program, Scientific Results Volume 204

16. Dissolved Fluoride Concentrations in Methane-Charged Sediment Sequences[1]

Gerald R. Dickens,[2] Catherine M. Donohue,[2] and Glen T. Snyder[2]

ABSTRACT

Dissolved fluoride was determined for pore waters at eight sites drilled on Hydrate Ridge during Ocean Drilling Program (ODP) Leg 204 and one site drilled in the Peru Trench during ODP Leg 201. All nine sites contain a shallow (<20 m) sulfate–methane transition (SMT) above abundant methane including gas hydrate. For Sites 1248, 1249, and 1250 on the crest of Hydrate Ridge, F^- concentrations are significantly lower than that of seawater in the shallowest samples (<50 µM), rise to a broad maximum, and generally decrease with depth. The low values at the top are consistent with rapid F^- removal at or near the seafloor, and the relatively smooth F^- profiles are consistent with high upward fluid fluxes. In contrast, Sites 1244, 1245, 1247, 1251, and 1252 from the flanks and slope basins of Hydrate Ridge and Site 1230 from the Peru Trench have F^- profiles apparently characterized by two lows with an intervening high. Processes involving sediment components appear to consume F^- at shallow depth, release F^- at intermediate depth, and consume F^- again at deeper depth. The upper low in F^- concentrations consistently lies near the SMT where pore water alkalinity and Mg^{2+} profiles suggest precipitation of Mg-rich carbonate. A similar pattern occurs at other sites drilled into methane-charged sediment. We speculate that Mg-rich carbonates (e.g., high-Mg calcite, protodolomite, and dolomite) remove F^- from pore water near the SMT but, with burial and recrystallization, return F^- to pore waters at depth. Authigenic Mg-rich carbonates conceivably represent a major sink of F^- from the ocean, although additional work is needed to confirm this idea.

[1] Dickens, G.R., Donohue, C.M., and Snyder, G.T., 2006. Dissolved fluoride concentrations in methane-charged sediment sequences. *In* Tréhu, A.M., Bohrmann, G., Torres, M.E., and Colwell, F.S. (Eds.), *Proc. ODP, Sci. Results,* 204, 1–22 [Online]. Available from World Wide Web: <http://www-odp.tamu.edu/publications/204_SR/VOLUME/CHAPTERS/118.PDF>. [Cited YYYY-MM-DD]
[2] Department of Earth Sciences, Rice University, Houston TX 77005, USA. Correspondence author: **jerry@rice.edu**

Initial receipt: 23 March 2005
Acceptance: 8 March 2006
Web publication: 29 September 2006
Ms 204SR-118

INTRODUCTION

Fluoride is a significant dissolved constituent in the oceans, having a concentration of 68 µM in seawater with salinity of 35‰ (e.g., Greenhalgh and Riley, 1961). Despite its high concentration, the large-scale geochemical cycling of F remains problematic (Rude and Aller, 1994). Rivers contribute nominally 16.8×10^{10} mol/yr of F to the oceans (Carpenter, 1969). Presumably, this input balances (or nearly balances) outputs to the seafloor. Various authors have identified and quantified a series of major F sinks, including authigenic carbonate fluorapatite (CFA), biogenic calcium carbonate, terrigenous aluminosilicate alteration, biogenic opal, and hydrothermal activity (e.g., Carpenter, 1969; Edmond et al., 1979; Froelich et al., 1983; Rude and Aller, 1994). However, these seafloor outputs amount to $<6.5 \times 10^{10}$ mol/yr of F, and some unidentified process seems to remove substantial F from the ocean (Rude and Aller, 1994).

Enormous quantities of methane reside as dissolved gas, gas hydrates, and free gas in the pore space of marine sediment along continental margins (Kvenvolden, 1999; Dickens, 2001). Crucially, this CH_4 is dynamic with clearly established (though poorly constrained) carbon fluxes between the ocean and sediment (Dickens, 2003). One ubiquitous flux is through anaerobic oxidation of methane (AOM). Above all methane-charged sediment sequences examined to date (e.g., Borowksi et al., 1999; D'Hondt et al., 2002), upward migrating CH_4 reacts with downward diffusing SO_4^{2-} at a sulfate–methane transition (SMT) to produce HCO_3^- and H_2S (Fig. **F1**). The SMT can occur at or beneath the seafloor. Importantly, removal of SO_4^{2-} and production of HCO_3^- leads to precipitation of authigenic carbonate minerals, especially Mg-rich phases such as high-Mg calcite (HMC), protodolomite, and dolomite (e.g., Ritger et al., 1987; Aloisi et al., 2000; Rodriguez et al., 2000; Greinert et al., 2001; Moore et al., 2004). The exact depth relationship between the SMT and the various authigenic Mg-rich carbonate minerals remains unclear and may vary from one location to another. Nonetheless, pore water profiles above methane-charged sediment systems invariably show concave-downward inflections in dissolved Ca^{2+} and dissolved Mg^{2+} (and inflections in alkalinity and Mg/Ca) consistent with Mg-rich carbonate formation near the SMT (Fig. **F1**). The overall process is intriguing to studies of the marine F cycle because F^- complexes with dissolved Mg^{2+} in seawater (e.g., Rude and Aller, 1991) and Mg-rich carbonates preferentially incorporate F (Akaiwa and Aizawa, 1979; Rude and Aller, 1991).

Rude and Aller (1991) show that dissolution of biogenic Mg-rich carbonate releases F^- to surrounding pore waters. To our knowledge, however, uptake of F^- into authigenic Mg-rich carbonates has not been considered, excepting a brief note by Schulz et al. (1994). In this study, we measure F^- concentrations of pore waters collected at nine drill sites that contain abundant methane, an SMT in shallow (<20 meters below seafloor [mbsf]) sediment, and evidence for methane-driven authigenic Mg-rich carbonate precipitation (D'Hondt, Jørgensen, Miller, et al., 2003; Tréhu, Bohrmann, Rack, Torres, et al., 2003). Sediments clearly remove F^- from pore water near the SMT, although additional work is needed to confirm that the F^- is entering authigenic Mg-rich carbonate.

F1. Pore water CH_4, SO_4^{2-}, alkalinity, Mg^{2+}, and Ca^{2+} profiles, p. 13.

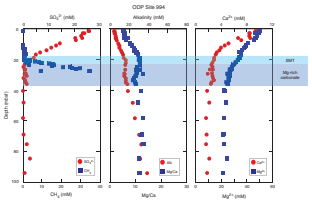

GEOCHEMICAL SETTING

The nine sites represent two significantly different geochemical environments. Sites 1248, 1249, and 1250 were drilled on the crest of Hydrate Ridge (Tréhu, Bohrmann, Rack, Torres, et al., 2003) in a region of active seafloor methane venting (e.g., Torres et al., 2002). Strong upward advection of fluids, both water and gas, characterizes these sites (Milkov et al., 2003; Tréhu, Bohrmann, Rack, Torres, et al., 2003; Torres et al., 2004). This high fluid flux impacts pore water geochemistry in three ways. First, massive amounts of gas hydrate occur in shallow sediment (Tréhu, Bohrmann, Rack, Torres, et al., 2003), and its formation and dissociation affect measured pore water concentrations (Milkov et al., 2004; Tréhu et al., 2004; Torres et al., 2004). Second, fluid advection rapidly transports deep formation water to shallow depth, which makes concentrations of various dissolved species relatively constant with respect to depth except within the uppermost few meters beneath the seafloor or in zones with massive gas hydrate (Tréhu, Bohrmann, Rack, Torres, et al., 2003; Torres et al., 2004). Third, the SMT lies within 1.2 m of the seafloor (Fig. **F2**). Not surprisingly, within the upper meter of sediment, pore water alkalinity and Mg/Ca are very high (>40 mM and 10, respectively), whereas pore water Ca and Mg are relatively low (<4 mM and 40 mM, respectively). Magnesium-rich carbonate must be precipitating at or near the seafloor. Indeed, numerous samples of HMC, protodolomite, and dolomite have been recovered from sediment on the crest of Hydrate Ridge (Greinert et al., 2001), and specimens of HMC were found in the upper 3 m at Sites 1248 and 1250 (**Teichert and Bohrmann,** this volume).

Other Leg 204 sites were drilled on the flanks (Sites 1244, 1245, and 1247) or surrounding slope basins (Sites 1251 and 1252) of Hydrate Ridge (Tréhu, Bohrmann, Rack, Torres, et al., 2003). Fluid flux at these sites is much weaker than at the crest of Hydrate Ridge. As a consequence, there is much less gas hydrate (Milkov et al., 2003; Tréhu et al., 2004), and many profiles of pore water chemistry display highs and lows in concentration separated by diffusion gradients (Tréhu, Bohrmann, Rack, Torres, et al., 2003). The peaks and troughs, which define changes in concentration gradient, represent zones where sedimentary components release or consume dissolved constituents. The SMT, characterized by a sharp change in the SO_4^{2-} gradient, occurs between 7.4 and 12.4 mbsf at the flank sites, and between 3.6 and 6.3 mbsf at the slope basin sites (Fig. **F2**). Dissolved Mg^{2+} concentrations were measured at all these sites except Site 1252 (Tréhu, Bohrmann, Rack, Torres, et al., 2003). Although the downhole Mg^{2+} profiles show scatter, concave-downward inflections in this species and the pore water Mg/Ca ratio generally occur in shallow sediment at or beneath the SMT (Fig. **F2**). Presumably, this change in slope marks a zone of Mg-carbonate precipitation near the SMT, as predicted from studies on Blake Ridge (Rodriguez et al., 2000) and elsewhere. Leg 204 shipboard X-ray diffraction (XRD) analyses confirmed massive dolomite between 9.1 and 9.4 mbsf at Site 1247 (Tréhu, Bohrmann, Rack, Torres, et al., 2003; **Teichert and Bohrmann,** this volume). Indurated horizons comprising low-magnesium calcite and HMC were also found at various depths at each of these sites (**Teichert and Bohrmann,** this volume). However, it is not yet clear when and where these carbonates formed. Some may be actively forming near the SMT; others may have precipitated in the past and been subsequently buried.

F2. Pore water SO_4^{2-}, F^-, alkalinity, and Mg/Ca profiles, p. 14.

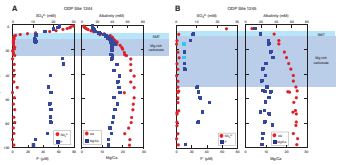

Pore water chemistry at Site 1230 in the Peru Trench has many similarities to flank sites of Hydrate Ridge, including the presence of scattered gas hydrate beneath 80 mbsf (cf. D'Hondt, Jørgensen, Miller, et al., 2003; Tréhu, Bohrmann, Rack, Torres, et al., 2003). Of interest to this investigation, a well-defined SMT occurs between 7.65 and 9.15 mbsf and pore water alkalinity and Mg/Ca show changes in slope at ~8 and ~35 mbsf (Fig. **F2**).

SAMPLE COLLECTION AND ANALYSES

Pore waters were collected during both legs according to standard procedures aboard the *JOIDES Resolution* (Gieskes et al., 1991; D'Hondt, Jørgensen, Miller, et al., 2003; Tréhu, Bohrmann, Rack, Torres, et al., 2003). Briefly, interstitial water (IW) samples were collected by squeezing whole-round sediment intervals and by filtering released water into plastic syringes. From IW samples with sufficient water, an aliquot was dispensed into a precleaned glass ampule for F^- analysis. Glass ampules were used because they were available. Although we recognize potential problems with storage in glass, resulting pore water F^- profiles exhibit smooth trends (Fig. **F2**), suggesting that any effects on F^- concentration are minimal. In total, 224 pore water samples were obtained from Sites 1244 through 1252, excluding Site 1246 (202 samples) and Site 1230 (22 samples). Samples from depth intervals containing massive gas hydrate (e.g., ~10 mbsf at Site 1249) (Milkov et al., 2004; Torres et al., 2004) were avoided.

Fluoride concentrations in pore waters were measured using an established colorimetric method (Greenhalgh and Riley, 1961), modified for small sample volumes (200 µL). In this method, F^- complexes with an alazarin lanthanum reagent, making a blue solution, where color intensity corresponds to F^- concentration. In brief, 1.07 mL of lanthanum alizarin complexone was mixed with 200 µL of sample and 1.8 mL of artificial seawater in a 3 mL cuvet. After 30 min, the cuvet was placed in a Varian ultraviolet-visible (UV-VIS) spectrometer and the absorbance of the sample was measured at 622 nm. The wavelength absorbance was converted to concentration using a curve constructed from standards of 0.25 ppm (13.16 µM), 0.20 ppm (10.53 µM), 0.15 ppm (7.89 µM), 0.10 ppm (5.26 µM), 0.05 ppm (2.63 µM), and 0.0 ppm. Samples of International Association for the Physical Sciences of the Oceans (IAPSO) water (diluted 1:50) and brackish water collected from the shore of Galveston Bay (diluted 1:10) were analyzed multiple times to evaluate accuracy and precision. These replicate analyses gave F^- concentrations of 1.2 ± 0.16 µM and 3.5 ± 0.26 µM, respectively. After correcting for dilution and considering the error, the IAPSO value of 61 µM compares favorably with the reported F^- value of 68–72 µM (e.g., Greenhalgh and Riley, 1961). There are no published values for F^- concentrations of water from Galveston Bay, but 35 µM (after correcting for dilution) seems reasonable given the low salinity of this water mass. A detection limit of 9 µM was also determined for the method. Other workers have used variations of this method to determine F^- concentrations in pore waters of marine sediment (e.g., Froelich et al., 1983; Jahnke et al., 1983; Schuffert et al., 1994), and a more detailed description is given in Donohue (2004).

RESULTS

Crest of Hydrate Ridge

Although sample resolution is low, dissolved F^- concentrations appear to exhibit similar depth profiles at the three sites on the crest of Hydrate Ridge (Table T1; Fig. F2). Samples within the upper 15 mbsf have fairly low F^- concentrations (<30 µM at Site 1249 and <40 µM at Site 1250). Concentrations rise to a broad high between 20 and 50 mbsf, depending on the site, and steadily decrease below. At Site 1248, F^- concentrations drop below detection at ~130 mbsf (Table T1; Fig. F3).

The generally smooth F^- profiles conform to downhole trends in other dissolved species, except where horizons contain massive gas hydrate (Tréhu, Bohrmann, Rack, Torres, et al., 2003). High rates of fluid advection likely "smooth" signatures associated with chemical reactions. Nonetheless, reactions involving F^- must occur in at least three horizons. The low F–concentrations of shallow samples (<1.1 mbsf) are much lower than that of seawater (68 µM), so some phase must remove substantial amounts of F^- at or near the seafloor. The broad F^- maximum indicates release of F^- to pore waters at depth. By contrast, the gradual decline in F^- with depth implies sequestration of F^- deeper in the sediment column.

Flanks and Slope Basins of Hydrate Ridge

The five sites from the flanks or slope basins of Hydrate Ridge also have broadly similar F^- profiles considering the limited sampling (Table T1; Fig. F2). Fluoride concentrations are relatively high in samples within 2.5 m of the seafloor. Indeed, Sample 204-1244C-1H-1, 65–75 cm, has a concentration (61 µM) close to that of seawater, especially given the accuracy of our method. Concentrations then drop to a minimum (<40 µM) that appears to begin near the SMT. Dissolved F^- remains low from 1 to 20 mbsf and then rises to a broad maximum somewhere between 25 and 80 mbsf, depending on location. The increase seems to begin where pore water alkalinity and Mg/Ca have secondary inflections. Deeper in the sediment, F^- concentrations generally decrease, dropping below detection somewhere between 110 and 250 mbsf at Sites 1244, 1245, 1251, and 1252 (Table T1; Fig. F3).

As for the crest of Hydrate Ridge, dissolved F^- profiles suggest that reactions involving F^- occur at three horizons. Components within the sediment appear to consume F^- at shallow depth, release F^- at intermediate depth, and sequester F^- again at deeper depth. In terms of overall F^- trends, the only distinctions from the crest sites are the high concentrations near the seafloor and the more pronounced peaks and troughs. These differences are probably explained by high advection rates on the crest of Hydrate Ridge and the general tendency for fluid flow to push chemical gradients toward the seafloor. In particular, a steep drop in F^- concentrations might occur within the upper few centimeters of sediment on the crest of Hydrate Ridge.

Peru Trench

With available sampling resolution, the dissolved F^- profile at Site 1230 is somewhat similar to those constructed for sites from the flanks or slope basins of Hydrate Ridge (Table T1; Fig. F2). Sample 201-1230A-

T1. Dissolved fluoride concentrations, p. 21.

F3. Pore water F^- profiles, p. 19.

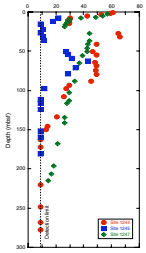

2H-5, 135–150 cm, at 12.15 mbsf and from several meters below the SMT has a F^- concentration (36 µM) significantly lower than that of seawater. From this depth, F^- concentrations appear to rise to a maximum of ~60 µM at ~40 mbsf and then steadily decrease to <20 µM by ~100 mbsf. Below 100 mbsf, F^- concentrations are generally <30 µM (Fig. F3).

DISCUSSION

Anaerobic oxidation of methane (AOM) in marine sediment increasingly has been recognized as a globally important biogeochemical process (Borowski et al., 1999; D'Hondt et al., 2002; Dickens, 2003). As this reaction simultaneously removes dissolved SO_4^{2-} and produces HCO_3^-, AOM can lead to precipitation of authigenic Mg-rich carbonates at and beneath the seafloor (Ritger et al., 1987; Aloisi et al., 2000; Rodriguez et al., 2000; Greinert et al., 2001; Moore et al., 2004). Such carbonates might preferentially incorporate F (Akaiwa and Aizawa, 1979), removing dissolved F^- from pore waters near the SMT.

Results presented in this study (Fig. F2) bolster this idea at a basic level. Sites 1249 and 1250 lie on the crest of Hydrate Ridge, where the SMT and Mg-rich carbonates exist at or near the seafloor (Greinert et al., 2001; Tréhu, Bohrmann, Rack, Torres, et al., 2003). These sites have dissolved F^- concentrations much lower than that of seawater near the sediment/water interface, presumably because authigenic mineral formation has removed substantial F^-. Sites from the flanks and slope basins of Hydrate Ridge display a prominent drop in dissolved F^- that begins near the SMT and where pore water profiles suggest a zone of Mg-rich carbonate formation. The same appears to be true at Site 1230 in the Peru Trench.

Removal of F^- from pore waters of marine sediment has often been ascribed to growth of authigenic CFA. No CFA has been identified in sediment at sites on Hydrate Ridge and in the Peru Trench (D'Hondt et al., 2003; Tréhu, Bohrmann, Rack, Torres, et al., 2003), and we argue that it does not form here. Carbonate fluorapatite has a generic formula as follows:

$$Ca_{10}(PO_4)_{6-x}(CO_3)_xF_{2+x}\ (x \le 1.5)$$

(e.g., Froelich et al., 1988). Its precipitation, therefore, should remove 1.3 to 3 times more PO_4^{3-} than F^- from surrounding pore water on a molar basis. Geochemical studies of cores straddling active CFA formation generally show this to be true, with prominent drops in both dissolved PO_4^{3-} and dissolved F^- (e.g., Jahnke et al., 1983; Froelich et al., 1988; Schuffert et al., 1994; Schenau et al., 2000). However, for sites on Hydrate Ridge and in the Peru Trench, dissolved PO_4^{3-} concentrations steadily increase across the low in dissolved F^- (Fig. F4), strongly suggesting that F enters a sedimentary phase containing little or no P. We further note the high alkalinity (>20 µM) and high Mg/Ca ratio across the SMT at all nine sites (Fig. F2). In general, high pore water alkalinity and Mg/Ca preclude formation of CFA (Jahnke et al., 1983; Schenau et al., 2000).

The broad maximum in pore water F^- concentrations from 25 to 80 m below the SMT (Fig. F2) suggests that F is released from sedimentary components to pore waters at depth. A generic explanation is that the metastable Mg-rich carbonates (e.g., HMC and protodolomite) that se-

F4. Pore water F^- and PO_4^{3-} profiles, p. 20.

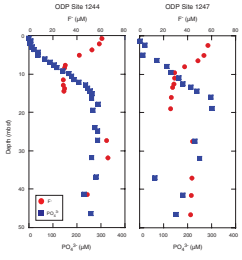

questered F^- at shallow depth return F to pore waters during burial and recrystallization. This concept is difficult to address because we know of no studies that have systematically documented authigenic carbonate diagenesis with compatible F measurements. However, dolomite generally loses trace elements with burial and recrystallization (e.g., Malone et al., 1994, 1996). Moreover, at Blake Ridge, Mg-rich carbonate initially formed at and below the SMT (~20 mbsf) (Fig. **F1**) seems to recrystallize to siderite between 40 and 100 mbsf. Although the mechanism remains unclear, two lines of evidence support this alteration. First, sediments between 40 and 100 mbsf contain abundant dolomite but no siderite, whereas those below 100 mbsf contain moderate siderite but little to no dolomite (Rodriguez et al., 2000). Second, the stable carbon isotope composition ($\delta^{13}C$) of dolomite increases from about –15‰ at 40 mbsf to 0‰ at 100 mbsf, the latter a value approaching the 5‰ value of siderite (Rodriguez et al., 2000).

Relatively few pore water F^- profiles have been published with which to compare and understand our results. Most literature on F^- concentrations in marine sediment pertains to piston and box cores where a SMT marking AOM was not penetrated (e.g., Froelich et al., 1983; Schuffert et al., 1994; Schenau et al., 2000) or cannot be assessed from available data (e.g., Jahnke et al., 1983; Rude and Aller, 1994; Reimers et al., 1996). To our knowledge, F^- concentrations have only been published for two piston cores that clearly cross a zone characterized by AOM (RC-23-06-4-17-PC2 offshore Peru, Froelich et al., 1988; GeoB 1401 offshore the Congo, Schulz et al., 1994). Consistent with profiles at Hydrate Ridge and in the Peru Trench (Fig. **F2**), dissolved F^- drops in both cores to a minimum (<40 µM) at or below the SMT. Froelich et al. (1983) noted that dolomite was probably precipitating near the SMT in core RC-23-06-4-17-PC2, and Schulz et al. (1994) mentioned that authigenic carbonate forming at the SMT might incorporate F^- (and Mn^{2+}) in Core GeoB 1401. However, F^- removal by authigenic Mg-rich carbonate formation was not discussed in either paper.

Fluoride has rarely been measured in pore waters from Ocean Drilling Program (ODP) sites (Leg 114, Ciesielski, Kristoffersen, et al., 1988; Leg 141, Behrmann, Lewis, Musgrave, et al., 1992; Leg 166, Eberli, Swart, Malone, et al., 1997; Leg 168, Mottl et al., 2000; Leg 169, Gieskes et al., 2002; Leg 169S, Mahn and Gieskes, 2001; Leg 178, Barker, Camerlenghi, Acton, et al., 1999). Of the available sites with F^- profiles, only a few sites were drilled into methane-charged sediment sequences with clearly defined SMTs in shallow sediment. These few sites, however, do support a link between AOM, Mg-rich carbonate precipitation, and F^- removal from pore waters.

Sites 860 and 861 were cored on the slope near the Chile triple junction (Behrmann, Lewis, Musgrave, et al., 1992). Although pore water sampling resolution is fairly low at both sites over the upper 100 mbsf, dissolved SO_4^{2-}, Mg^{2+}, and F^- concentrations exhibit trends somewhat similar to those observed for slope basins of Hydrate Ridge (n.b. an incorrect F^- profile is shown for Site 861 by Behrmann, Lewis, Musgrave, et al., 1992). Dissolved F^- and Mg^{2+} decrease to lows (F^- = <45 µM at Site 860) across a shallow SMT, suggesting incorporation into Mg-rich carbonate. Fluoride then rises to a broad maximum at ~50 mbsf and slowly decreases toward the base of cored intervals. The F^- profiles were attributed to authigenic mineral formation but without specifics (Behrmann, Lewis, Musgrave, et al., 1992).

Sites 1095, 1096, and 1101 on the slope off the Antarctic Peninsula have deep SMTs at ~50, ~160, and ~120 mbsf, respectively (Barker, Camerlenghi, Acton, et al., 1999). Dissimilar to locations on Hydrate Ridge and in the Peru Trench, dissolved Mg^{2+} profiles at each of these sites display a concave-downward inflection 10 to 50 m above the SMT. The decreases in Mg^{2+} were attributed to clay diagenesis, although precipitation of authigenic Mg-rich carbonate was not dismissed (Barker, Camerlenghi, Acton, et al., 1999). Dissolved F^- generally decreases in tandem with Mg^{2+} at all three sites; however, unlike sites examined in our study, dissolved PO_4^{3-} also drops with increasing depth. Thus, removal of F^- was attributed to formation of CFA (Barker, Camerlenghi, Acton, et al., 1999). However, the drops in dissolved F^- (>60 µM) are much greater than the drops in dissolved PO_4^{3-} (<10 µM), suggesting that F^- and PO_4^{3-} are not entering a phase containing fewer moles of F than P (i.e., CFA).

Site 1098 in Palmer Deep has an SMT at ~29 mbsf (Barker, Camerlenghi, Acton, et al., 1999). Within a few meters above this interface, dissolved Ca^{2+} and Mg^{2+} both drop by 8–10 µM, strongly suggesting the formation of authigenic dolomite (Barker, Camerlenghi, Acton, et al., 1999). A prominent low in dissolved F^- (~10 µM) precisely coincides with this horizon. Again, however, removal of pore water F^- was attributed to CFA precipitation (Barker, Camerlenghi, Acton, et al., 1999), in this case despite rapidly increasing PO_4^{3-} concentrations across the SMT, similar to observations at Hydrate Ridge (Fig. **F3**).

SUMMARY AND FUTURE WORK

Sediment sequences on many continental margins contain large, dynamic CH_4 reservoirs. Methane migrating upward from these systems consumes pore water SO_4^{2-} across an SMT through AOM, a reaction that generates alkalinity and leads to precipitation of authigenic Mg-rich carbonates. Existing data, albeit limited, show that dissolved F^- concentrations decrease to local lows at or near the SMT in methane-charged sediment sequences. The loss of F^- from pore waters is not consistent with formation of CFA. We therefore suggest that authigenic Mg-rich carbonate precipitation removes significant amounts of dissolved F^-. However, at least three basic findings are required to confirm this hypothesis and, ultimately, whether authigenic Mg-rich carbonates provide a major sink of F from the ocean.

1. Dissolved F^- profiles at sites from Hydrate Ridge and the Peru Trench (Fig. **F2**) are not very detailed, principally because sample collection for F^- analyses was given low priority. High-resolution sampling of pore waters for F^- analyses is needed across the SMT and zones of Mg-carbonate precipitation at multiple sites.
2. Precipitation of Mg-rich carbonate at sites from Hydrate Ridge and the Peru Trench is largely inferred from pore water alkalinity and Mg^{2+} concentrations, as well as from information gleaned at other locations (e.g., Rodriguez et al., 2000). Chemical and mineralogical analyses of sediment are needed to show the presence of authigenic Mg-rich carbonate at and beneath the SMT. Moreover, dissolution or recrystallization of Mg-rich carbonate needs to be established if this mechanism is to offered as an explanation for the increase in dissolved F^- at intermediate depths.

3. Incorporation of F into Mg-rich carbonate implies that such carbonates contain elevated F contents soon after precipitation. In our literature searches, however, we can find no measurements of F in examples of authigenic carbonates from modern seafloor sediment (excluding CFA).

ACKNOWLEDGMENTS

This research used samples and/or data provided by the Ocean Drilling Program (ODP). ODP is sponsored by the U.S. National Science Foundation (NSF) and participating countries under management of Joint Oceanographic Institutions (JOI), Inc. Funding for this research was furnished by JOI/USSAC following participation of G. Dickens on ODP Leg 201. We gratefully acknowledge the support of this program, the captains and crews of ODP Legs 201 and 204, and the work of the shipboard geochemistry groups. We also thank the reviewers, M. Malone and S. Kasten, who offered very constructive comments and criticism (in full awareness of shortfalls in our manuscript), and the editorial staff at IODP.

REFERENCES

Akaiwa, H., and Aizawa, S., 1979. Fluorine contents of Permian carbonate rocks in central Japan. *Chem. Geol.,* 27:157–169. doi:10.1016/0009-2541(79)90110-4

Aloisi, G., Pierre, C., Rouchy, J.-M., Foucher, J.-P., Woodside, J., and the MEDINAUT Scientific Party, 2000. Methane-related authigenic carbonates of eastern Mediterranean Sea mud volcanoes and their possible relation to gas hydrate destabilization. *Earth Planet. Sci. Lett.,* 184:321–338. doi:10.1016/S0012-821X(00)00322-8

Barker, P.F., Camerlenghi, A., Acton, G.D., et al., 1999. *Proc. ODP, Init. Repts.,* 178 [Online]. Available from World Wide Web: <http://www-odp.tamu.edu/publications/178_IR/178TOC.HTM>.

Behrmann, J.H., Lewis, S.D., Musgrave, R.J., et al., 1992. *Proc. ODP, Init. Repts.,* 141: College Station, TX (Ocean Drilling Program).

Borowski, W.S., Paull, C.K., and Ussler, W., III, 1999. Global and local variations of interstitial sulfate gradients in deep-water, continental margin sediments: sensitivity to underlying methane and gas hydrates. *Mar. Geol.,* 159:131–154. doi:10.1016/S0025-3227(99)00004-3

Carpenter, R., 1969. Factors controlling the marine chemistry of fluorine. *Geochem. Cosmochim. Acta,* 33:1153–1167. doi:10.1016/0016-7037(69)90038-6

Ciesielski, P.F., Kristoffersen, Y., et al., 1988. *Proc. ODP, Init. Repts.,* 114: College Station, TX (Ocean Drilling Program).

Dickens, G.R., 2001. The potential volume of oceanic methane hydrates with variable external conditions. *Org. Geochem.,* 32:1179–1193. doi:10.1016/S0146-6380(01)00086-9

Dickens, G.R., 2003. Rethinking the global carbon cycle with a large, dynamic and microbially mediated gas hydrate capacitor. *Earth Planet. Sci. Lett.,* 213(3–4):169–183. doi:10.1016/S0012-821X(03)00325-X

D'Hondt, S.L., Jørgensen, B.B., Miller, D.J., et al., 2003. *Proc. ODP, Init. Repts.,* 201 [Online]. Available from World Wide Web: <http://www-odp.tamu.edu/publications/201_IR/201ir.htm>.

D'Hondt, S.D., Rutherford, S., and Spivack., A.J., 2002. Metabolic activity of the subsurface biosphere in deep-sea sediments. *Science,* 295:2067–2070. doi:10.1126/science.1064878

Donohue, C.M., 2004. Regulation of fluorine chemistry and carbonate fluorapatite stability in deep sediments near the Peruvian upwelling zone [M.Sc. thesis]. Rice Univ., Houston.

Eberli, G.P., Swart, P.K., Malone, M.J., et al., 1997. *Proc. ODP, Init. Repts.,* 166: College Station, TX (Ocean Drilling Program). [HTML]

Edmond, J.M., Measures, C., McDuff, R.E., Chan, L.H., Collier, R., and Grant, B., 1979. Ridge crest hydrothermal activity and the balances of the major and minor elements in the ocean: the Galapagos data. *Earth Planet. Sci. Lett.,* 46:1–18.

Froelich, P.N., Arthur, M.A., Burnett, W.C., Deakin, M., Hensley, V., Jahnke, R., Kaul, L., Kim, K.H., Roe, K., Soutar, A., and Vathakanon, C., 1988. Early diagenesis of organic matter in Peru margin sediments: phosphorite precipitation. *Mar. Geol.,* 80:309–343. doi:10.1016/0025-3227(88)90095-3

Froelich, P.N., Kim, K.K., Jahnke, R.J., Burnett, W.R., Soutar, A., and Deakin, M., 1983. Pore water fluoride in Peru continental margin sediments: uptake from seawater. *Geochim. Cosmochim. Acta,* 47:1605–1612. doi:10.1016/0016-7037(83)90187-4

Gieskes, J.M., Gamo, T., and Brumsack, H., 1991. Chemical methods for interstitial water analysis aboard *JOIDES Resolution. ODP Tech. Note,* 15 [Online]. Available from World Wide Web: <http://www-odp.tamu.edu/publications/tnotes/tn15/f_chem1.htm>.

Gieskes, J.M., Simoneit, B.R.T., Goodfellow, W.D., Baker, P.A., and Mahn, C., 2002. Hydrothermal geochemistry of sediments and pore waters in Escanaba Trough—ODP Leg 169. *Appl. Geochem.,* 17:1435–1456. doi:10.1016/S0883-2927(02)00111-7

Greenhalgh, R., and Riley, J.P., 1961. The determination of fluoride in natural waters, with particular reference to seawater. *Anal. Chim. Acta,* 25:179–188. **doi:10.1016/S0003-2670(01)81541-5**

Greinert, J., Bohrmann, G., and Suess, E., 2001. Gas hydrate-associated carbonates and methane-venting at Hydrate Ridge: classification, distribution and origin of authigenic lithologies. *In* Paul, C.K., and Dillon, W.P. (Eds.), *Natural Gas Hydrates: Occurrence, Distribution, and Detection*. Geophys. Monogr., 124:99–114.

Jahnke, R.A., Emerson, S.R., Roe, K.K., and Burnett, W.C., 1983. The present day formation of apatite in Mexican continental margin sediments. *Geochim. Cosmochim. Acta,* 47:259–266. **doi:10.1016/0016-7037(83)90138-2**

Kvenvolden, K.A., 1999. Potential effects of gas hydrate on human welfare. *Proc. Natl. Acad. Sci. U. S. A.,* 96:3420–3426.

Mahn, C.L., and Gieskes, J.M., 2001. Halide systematics in comparison with nutrient distributions in Sites 1033B and 1034B, Saanich Inlet: ODP 169S. *In* Bornhold, B.D., and Kemp, A.E.S. (Eds.), *Late Quaternary Sedimentation in Saanich Inlet, British Columbia, Canada—Ocean Drilling Program Leg 169S*. Mar. Geol., 174:323–339. **doi:10.1016/S0025-3227(00)00158-4**

Malone, M.J., Baker, P.A., and Burns, S.J., 1994. Recrystallization of dolomite: evidence from the Monterey Formation (Miocene), California. *Sedimentology,* 41:1123–1239. **doi:10.1111/j.1365-3091.1994.tb01450.x**

Malone, M.J., Baker, P.A., and Burns, S.J., 1996. Recrystallization of dolomite: an experimental study from 50–200 degrees C. *Geochim. Cosmochim. Acta,* 60:2189–2207. **doi:10.1016/0016-7037(96)00062-2**

Milkov, A.V., Claypool, G.E., Lee, Y-J., Xu, W., Dickens, G.R., Borowski, W.S., and the ODP Leg 204 Scientific Party, 2003. In situ methane concentrations at Hydrate Ridge offshore Oregon: new constraints on the global gas hydrate inventory from an active margin. *Geology,* 31:833–836.

Milkov, A.V., Dickens, G.R., Claypool, G.E., Lee, Y-J., Borowski, W.S., Torres, M.E., Xu, W., Tomaru, H., Tréhu, A.M., and Schultheiss, P., 2004. Co-existence of gas hydrate, free gas, and brine within the regional gas hydrate stability zone at Hydrate Ridge (Oregon margin): evidence from prolonged degassing of a pressurized core. *Earth Planet. Sci. Lett.,* 222:829–843. **doi:10.1016/j.epsl.2004.03.028**

Moore, T.S., Murray, R.W., Kurtz, A.C., and Schrag, D.P., 2004. Anaerobic methane oxidation and the formation of dolomite. *Earth Planet. Sci. Lett.,* 229:141–154. **doi:10.1016/j.epsl.2004.10.015**

Mottl, M.J., Wheat, C.G., Monnin, C., and Elderfield, H., 2000. *Data report:* Trace elements and isotopes in pore water from Sites 1023 through 1032, eastern flank of the Juan de Fuca Ridge. *In* Fisher, A., Davis, E.E., and Escutia, C. (Eds.), *Proc. ODP, Sci. Results,* 168: College Station, TX (Ocean Drilling Program), 105–115. [**HTML**]

Paull, C.K., Matsumoto, R., Wallace, P.J., et al., 1996. *Proc. ODP, Init. Repts.,* 164: College Station, TX (Ocean Drilling Program).

Reimers, C.E., Ruttenberg, K.C., Canfield, D.E., Christiansen, M.B., and Martin, J.B., 1996. Porewater pH and authigenic phases formed in the uppermost sediments of the Santa Barbara Basin. *Geochim. Cosmochim. Acta,* 60:4037–4057. **doi:10.1016/S0016-7037(96)00231-1**

Ritger, S., Carson, B., and Suess, E., 1987. Methane-derived authigenic carbonates formed by subduction-induced pore-water expulsion along the Oregon/Washington margin. *Geol. Soc. Am. Bull.,* 98:147–156.

Rodriguez, N.M., Paull, C.K., and Borowski, W.S., 2000. Zonation of authigenic carbonates within gas hydrate-bearing sedimentary sections on the Blake Ridge: offshore southeastern North America. *In* Paull, C.K., Matsumoto, R., Wallace, P.J., and Dillon, W.P. (Eds.), *Proc. ODP, Sci. Results,* 164: College Station, TX (Ocean Drilling Program), 301–312. [**HTML**]

Rude, P.D., and Aller, R.C., 1991. Fluorine mobility during early diagenesis of carbonate sediment: an early indicator of mineral transformations. *Geochim. Cosmochim. Acta,* 55:2491–2509. **doi:10.1016/0016-7037(91)90368-F**

Rude, P.D., and Aller, R.C., 1994. Fluorine uptake by Amazon continental shelf sediment and its impact on the global fluorine cycle. *Cont. Shelf Res.,* 14:883–907. **doi:10.1016/0278-4343(94)90078-7**

Schenau, S.J., Slomp, C.P., and DeLange, G.J., 2000. Phosphogenesis and active phosphorite formation in sediments from the Arabian Sea oxygen minimum zone. *Mar. Geol.,* 169:1–20. **doi:10.1016/S0025-3227(00)00083-9**

Schuffert, J.D., Jahnke, R.A., Kastner, M., Leather, J., Sturz., A., and Wing, M.R., 1994. Rates of formation of modern phosphorite off western Mexico. *Geochim. Cosmochim. Acta,* 58:5001–5010. **doi:10.1016/0016-7037(94)90227-5**

Schulz, H.D., Dahmke, A., Schinzel, U., Wallmann, K., and Zabel, M., 1994. Early diagenetic processes, fluxes, and reaction rates in sediments of the South Atlantic. *Geochim. Cosmochim. Acta,* 58:2041–2060. **doi:10.1016/0016-7037(94)90284-4**

Torres, M.E., McManus, J., Hammond, D.E., de Angelis, M.A., Heeschen, K.U., Colbert, S.L., Tryon, M.D., Brown, K.M., and Suess, E., 2002. Fluid and chemical fluxes in and out of sediments hosting methane hydrate deposits on Hydrate Ridge. *Earth Planet. Sci. Lett.,* 201:525–540. **doi:10.1016/S0012-821X(02)00733-1**

Torres, M.E., Wallmann, K., Tréhu, A.M., Bohrmann, G., Borowski, W.S., and Tomaru, H., 2004. Gas hydrate growth, methane transport, and chloride enrichment at the southern summit of Hydrate Ridge, Cascadia margin off Oregon. *Earth Planet. Sci. Lett.,* 226:225–241. **doi:10.1016/j.epsl.2004.07.029**

Tréhu, A.M, Bohrmann, G., Rack, F.R., Torres, M.E., et al., 2003. *Proc. ODP, Init. Repts.,* 204 [Online]. Available from World Wide Web: <**http://www-odp.tamu.edu/publications/204_IR/204ir.htm**>.

Tréhu, A.M., Long, P.E., Torres, M.E., Bohrmann, G., Rack, F.R., Collett, T.S., Goldberg, D.S., Milkov, A.V., Riedel, M., Schultheiss, P., Bangs, N.L., Barr, S.R., Borowski, W.S., Claypool, G.E., Delwiche, M.E., Dickens, G.R., Gracia, E., Guerin, G., Holland, M., Johnson, J.E., Lee, Y.-J., Liu, C.-S., Su, X., Teichert, B., Tomaru, H., Vanneste, M., Watanabe, M., and Weinberger, J.L., 2004. Three-dimensional distribution of gas hydrate beneath southern Hydrate Ridge: constraints from ODP Leg 204. *Earth Planet. Sci. Lett.,* 222:845–862. **doi:10.1016/j.epsl.2004.03.035**

Figure F1. Pore water CH_4, SO_4^{2-}, alkalinity, Mg^{2+}, and Ca^{2+} profiles at ODP Site 994, outer Blake Ridge (Paull, Matsumoto, Wallace, et al., 1996). Note the convergence of linear CH_4 and SO_4^{2-} profiles at the sulfate–methane transition (SMT) and the drops in alkalinity, Mg^{2+}, and Mg/Ca beneath the SMT. This zone contains authigenic Mg-rich carbonate, specifically dolomite at Site 994 (Rodriguez et al., 2000).

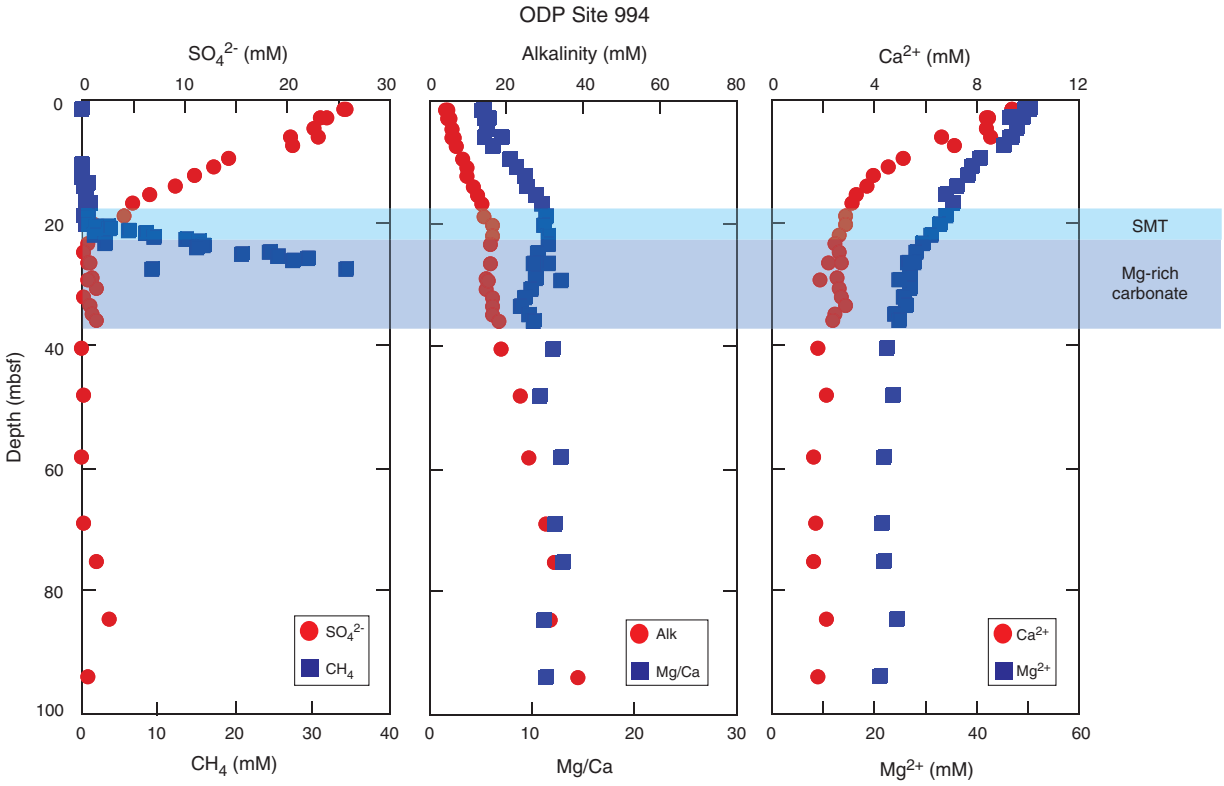

Figure F2. Pore water SO_4^{2-}, F^-, alkalinity, and Mg/Ca profiles at sites from Hydrate Ridge and the Peru Trench. The sulfate–methane transition (SMT) has been placed around the horizon where SO_4^{2-} drops to zero and alkalinity shows a concave-downward inflection. Following work on Blake Ridge, the inferred zone of Mg-rich carbonate formation is placed from the SMT to where alkalinity and Mg/Ca display secondary inflections. Note the general correspondence between the F^- low and the inferred zone of Mg-rich carbonate precipitation. **A.** Site 1244. **B.** Site 1245. (Continued on next four pages.)

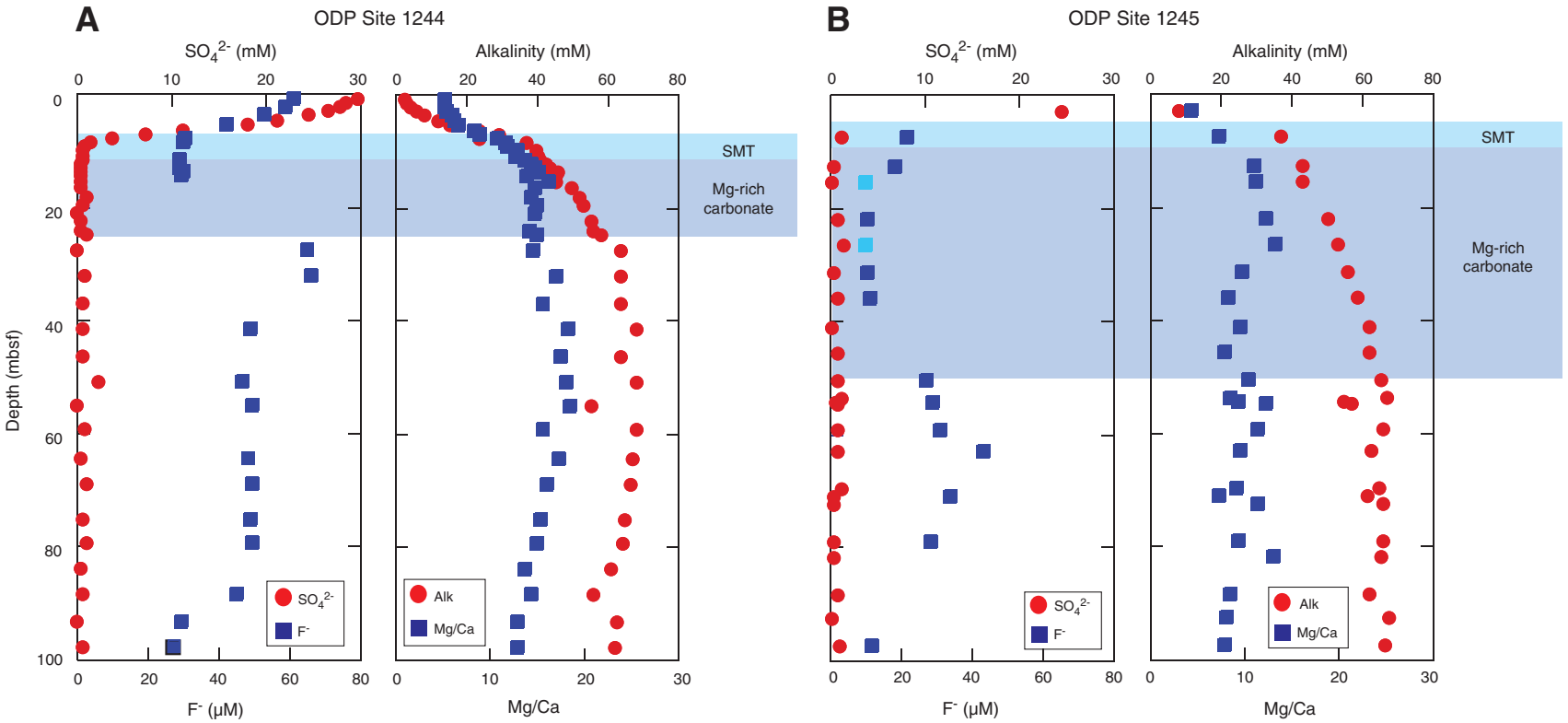

Figure F2 (continued). **C.** Site 1247. **D.** Site 1248. Arrow = depth where authigenic dolomite was documented. (Continued on next page.)

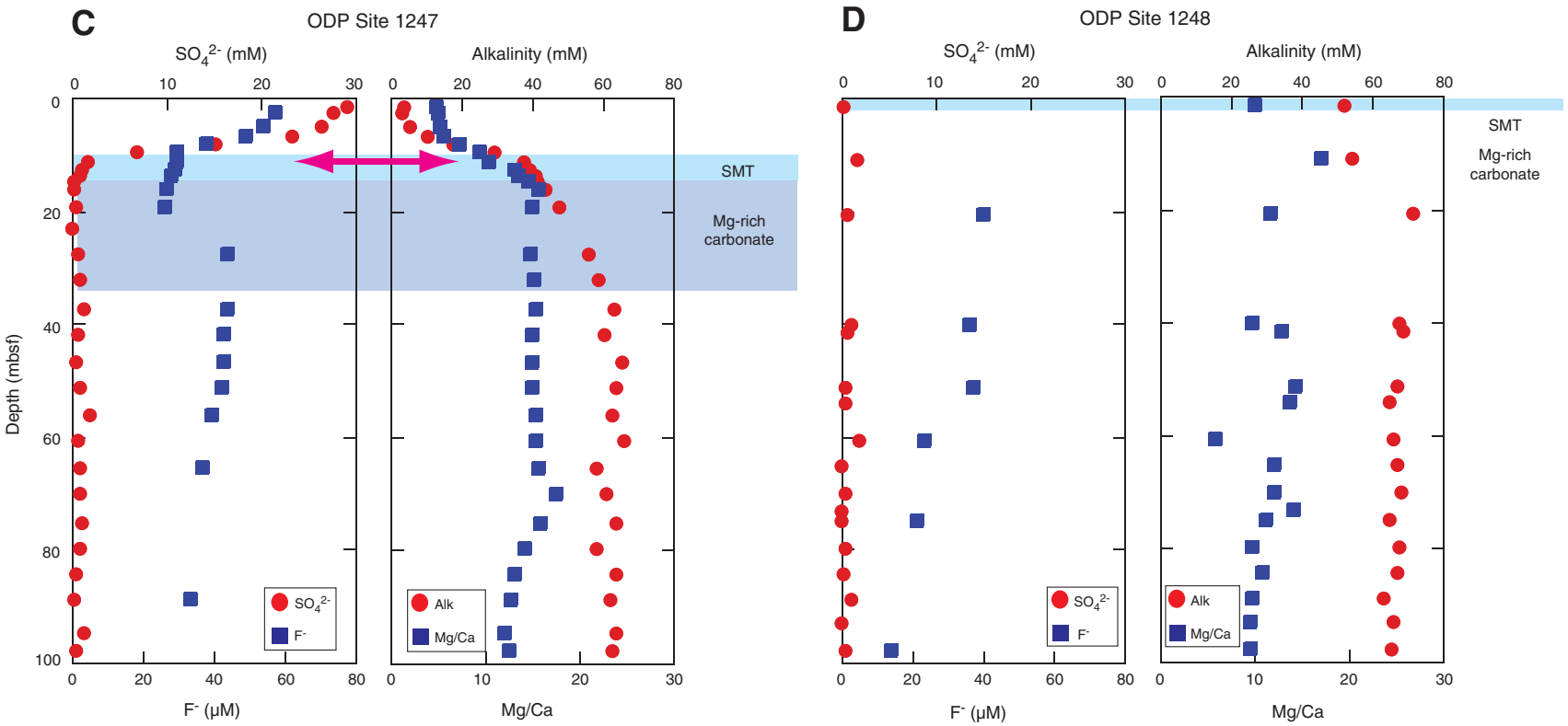

Figure F2 (continued). E. Site 1249. F. Site 1250. (Continued on next page.)

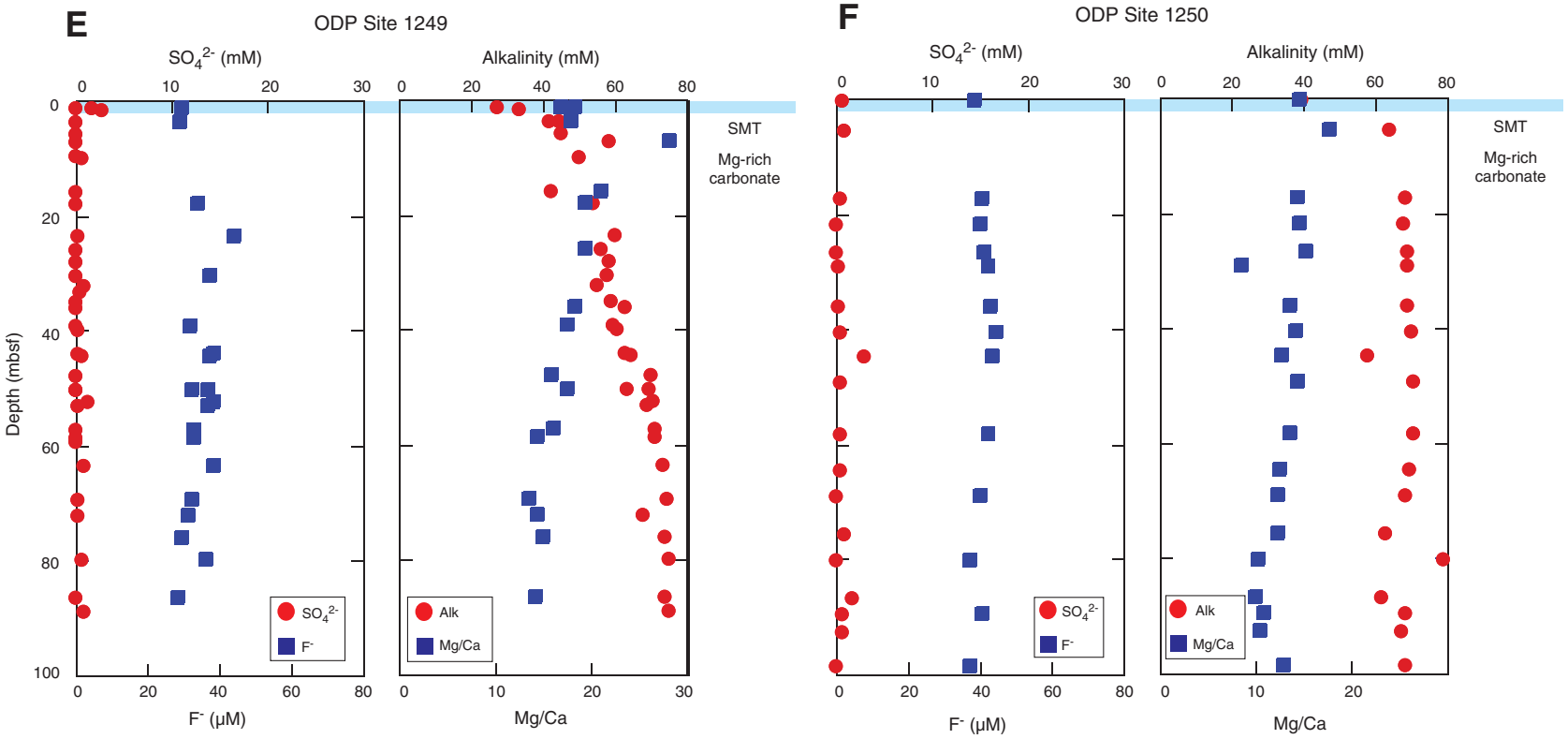

Figure F2 (continued). **G.** Site 1251. **H.** Site 1252. (Continued on next page.)

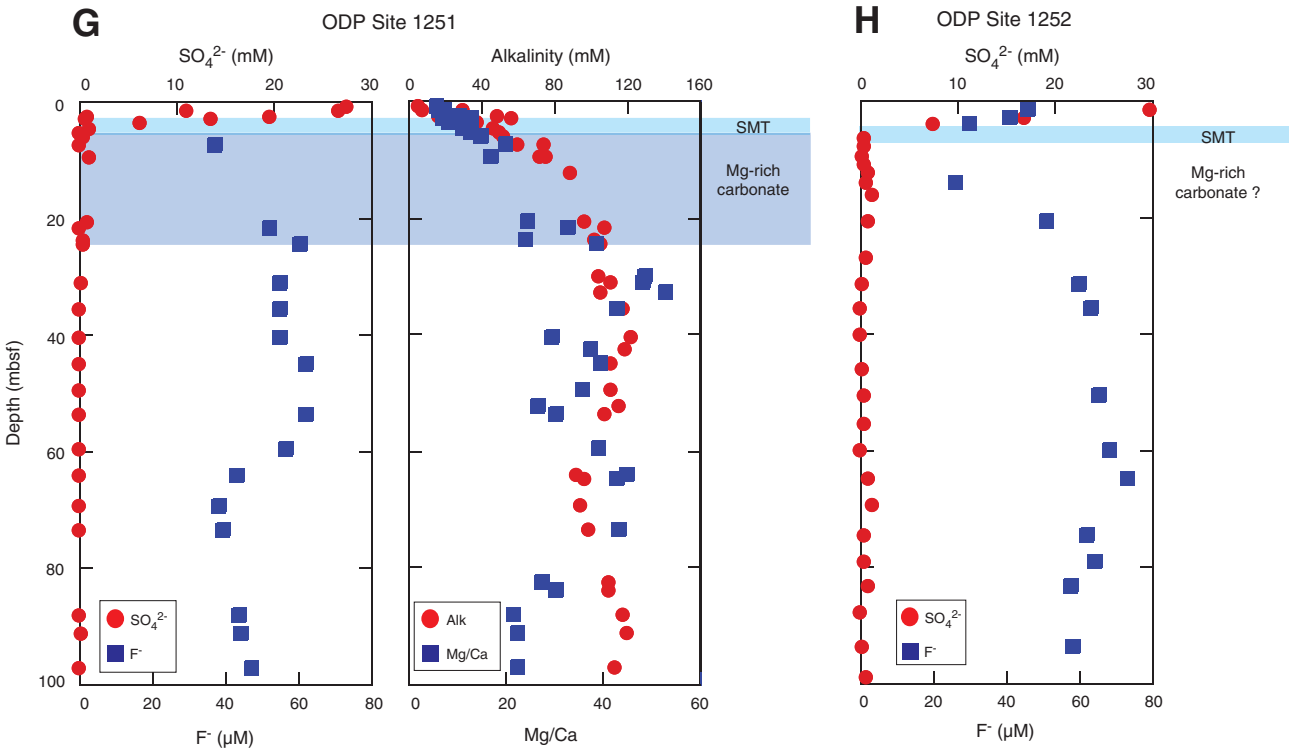

Figure F2 (continued). I. Site 1230.

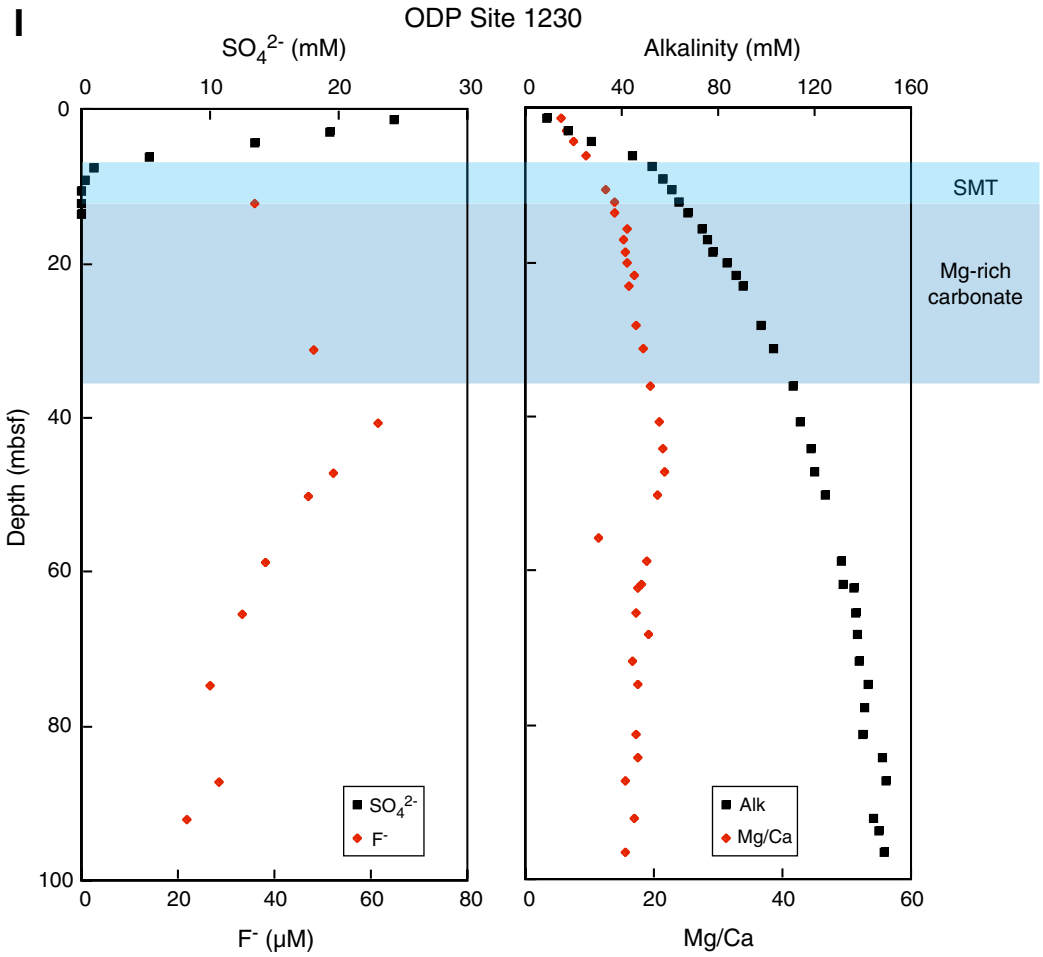

Figure F3. Pore water F^- profiles for the upper 300 mbsf at Sites 1244, 1245, and 1247. Note low F^- concentrations in sediment toward the bottom of holes at these sites.

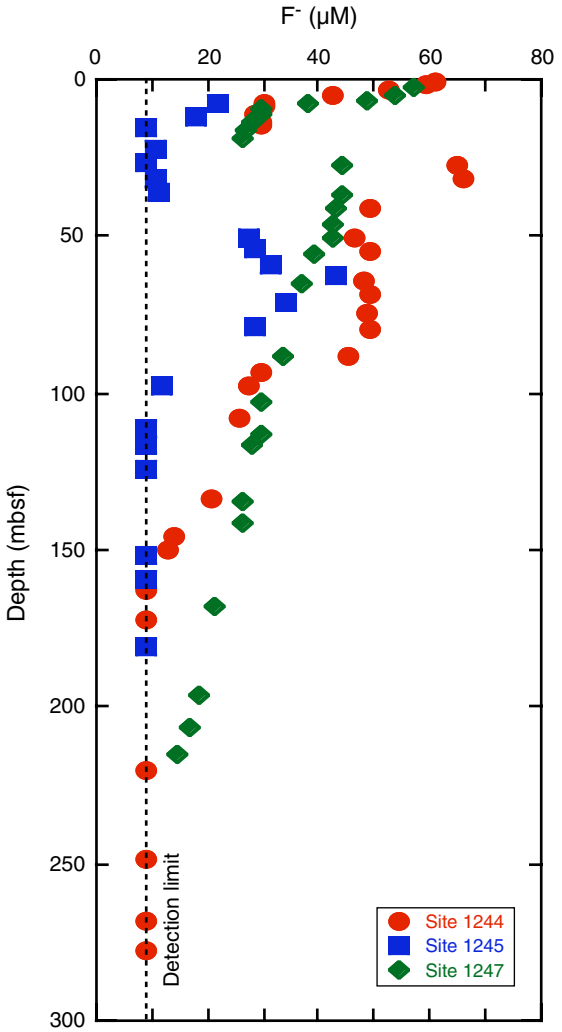

Figure F4. Pore water F^- and PO_4^{3-} profiles in the upper 50 m at ODP Sites 1244 and 1247. Note the rapidly increasing dissolved PO_4^{3-} across the SMT and low in dissolved F^-.

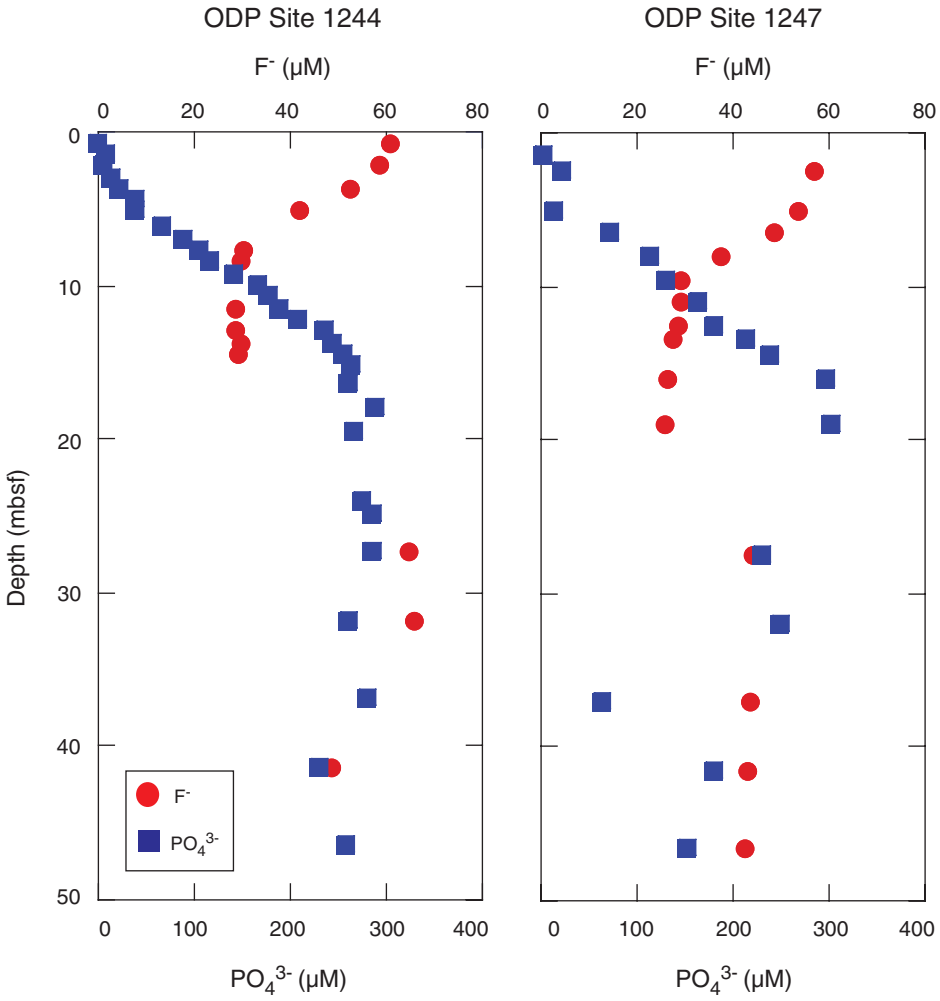

Table T1. Dissolved fluoride concentrations of pore waters from Hydrate Ridge and the Peru Trench. (See table notes. Continued on next page.)

Core, section, interval (cm)	Depth (mbsf)	F (μM)
204-1244C-		
1H-1, 65–75	0.65	61.0
1H-2, 65–75	2.15	59.1
1H-3, 65–75	3.65	52.7
1H-4, 60–70	5.10	42.4
2H-2, 65–75	7.65	30.4
2H-2, 140–150	8.40	30.0
2H-4, 140–150	11.40	28.8
2H-5, 140–150	12.90	29.0
2H-6, 65–75	13.65	29.9
2H-6, 140–150	14.40	29.7
4H-2, 135–150	27.35	65.1
4H-5, 135–150	31.85	66.0
5H-5, 135–150	41.35	49.1
6H-5, 135–150	50.71	46.6
7H-2, 135–150	54.79	49.5
8H-2, 135–150	64.37	48.1
8H-5, 135–150	68.87	49.3
9H-2, 135–150	74.85	48.9
9H-5, 135–150	79.35	49.3
10H-5, 135–150	88.38	45.2
11H-2, 135–150	93.08	29.6
11H-5, 135–150	97.58	27.5
12H-5, 135–150	107.85	26.0
17H-2, 30–45	133.70	20.9
19X-2, 135–150	145.85	14.0
19X-5, 85–100	149.85	12.9
21X-3, 135–150	163.15	BDL
22X-3, 135–150	172.65	BDL
27X-3, 130–150	220.10	BDL
30X-3, 130–150	249.00	BDL
32X-3, 130–150	268.24	BDL
33X-3, 130–150	277.84	BDL
36X-3, 130–150	306.90	BDL
204-1245B-		
1H-5, 140–150	7.40	21.7
2H-2, 140–150	12.40	18.2
2H-4, 140–150	15.40	BDL
3H-2, 140–150	21.90	10.6
3H-5, 140–150	26.40	BDL
4H-2, 140–150	31.40	10.6
4H-5, 140–150	35.90	11.4
6H-2, 140–150	50.40	27.2
6H-5, 78–88	54.28	28.8
7H-2, 140–150	58.95	31.1
7H-5, 140–150	62.98	43.3
8H-3, 140–150	70.82	34.0
9H-2, 134–144	78.66	28.6
11H-2, 140–150	97.37	11.9
12H-5, 140–150	111.87	BDL
13H-2, 111–126	116.61	BDL
14H-1, 125–140	123.95	BDL
18X-2, 113–138	151.73	BDL
19X-2, 125–150	159.75	BDL
21X-4, 77–102	181.27	BDL
204-1247B-		
1H-2, 90–100	2.40	57.0
2H-1, 140–150	5.00	54.0
2H-2, 140–150	6.50	48.7
2H-3, 140–150	8.00	38.0
2H-4, 140–150	9.50	29.7
2H-5, 140–150	11.00	29.7
2H-6, 140–150	12.50	28.8
2H-7, 77–87	13.37	27.9
3H-2, 140–150	16.00	26.6
3H-4, 140–150	19.00	26.1
5H-2, 140–150	27.50	44.2
6H-2, 140–150	37.00	44.0
6H-5, 140–150	41.50	43.1
7H-2, 140–150	46.45	42.6
7H-5, 140–150	50.95	42.3
8H-2, 140–150	56.00	39.3
9H-2, 140–150	65.41	36.9
11H-5, 140–150	88.61	33.5
13H-2, 140–150	103.13	29.9
14H-5, 62–83	113.32	29.5
15X-2, 135–150	116.45	28.1
18X-5, 135–150	134.65	26.1
19X-5, 130–150	141.87	26.2
22X-3, 130–150	167.80	21.1
25X-3, 130–150	196.33	18.5
26X-3, 130–150	206.20	16.8
27X-3, 130–150	215.50	14.8
204-1248C-		
3X-1, 140–150	20.60	40.0
5X-1, 140–150	39.80	35.9
6H-3, 129–139	51.05	37.3
7H-2, 140–150	60.40	23.6
8H-CC, 0–10	74.65	21.1
11H-2, 135–150	97.51	13.8
12H-5, 135–150	111.96	13.6
13H-4, 132–147	120.21	13.0
14H-2, 135–150	125.62	12.5
15H-2, 85–100	135.30	BDL
16H-1, 135–150	137.85	BDL
16H-3, 135–150	140.85	BDL
17X-1, 130–150	143.30	BDL
17X-3, 135–150	146.30	BDL
204-1249B-		
2A-1, 45–60	30.35	37.2
5A-1, 78–93	44.18	37.3
6A-2, 95–106	49.85	36.7
7A-1, 42–57	52.82	36.6
204-1249C-		
1H-1, 110–118	1.10	29.7
2H-2, 0–15	3.40	29.1
4H-5, 86–101	17.61	34.0
7H-5, 76–91	38.89	31.8
8H-4, 124–139	50.18	32.5
9H-2, 133–148	56.83	32.8
9H-3, 120–135	58.18	32.8
11H-4, 104–119	69.17	32.0
11H-6, 95–115	71.87	31.2
12H-1, 120–140	75.70	29.4
13H-2, 79–99	86.29	28.3
204-1249F-		
7H-2, 106–116	23.41	43.8
9H-3, 140–150	43.61	38.5
10H-2, 140–150	52.09	38.5
12H-2, 131–146	63.20	38.5
15H-5, 135–150	79.57	36.3
204-1250C-		
1H-1, 0–10	0.10	38.4
3H-2, 140–150	16.90	40.7
3H-5, 140–150	21.40	40.1
4H-2, 140–150	26.40	41.3
4H-4, 140–150	29.00	42.2
5H-2, 140–150	35.88	43.0
5H-5, 133–143	40.31	44.2
6H-2, 57–67	44.57	43.2
7H-5, 130–140	58.00	42.0
8H-5, 140–150	68.90	39.9
10H-5, 135–150	79.81	37.4

Table T1 (continued).

Core, section, interval (cm)	Depth (mbsf)	F (μM)
11H-5, 130–145	89.31	40.5
12H-5, 140–155	98.43	37.3
13H-2, 130–150	103.19	35.7
13H-5, 130–150	107.69	35.3
15H-1, 106–126	121.56	33.1
15H-4, 100–120	125.86	33.2
17H-1, 130–150	133.30	32.5
17H-3, 130–150	136.30	32.9
19X-2, 130–150	141.30	31.3
19X-5, 130–150	145.75	30.3
204-1251B-		
1H-5, 145–150	7.45	37.0
3H-2, 140–150	21.43	52.5
3H-4, 140–150	24.41	60.6
4H-2, 140–150	31.00	54.8
4H-5, 140–150	35.50	55.3
5H-2, 131–141	40.41	54.8
5H-5, 138–150	44.84	62.4
6H-5, 131–141	53.61	62.3
7H-2, 140–150	59.50	56.6
7H-5, 140–150	64.00	43.2
8H-2, 140–150	69.00	38.1
8H-5, 140–150	73.38	39.5
10H-2, 140–150	88.00	44.0
10H-4, 140–150	91.00	44.7
11H-2, 74–94	96.84	47.4
11H-5, 70–90	100.61	47.1
13H-2, 130–150	108.55	44.5
13H-5, 130–150	112.85	42.9
14H-2, 130–150	117.91	42.3
14H-5, 130–150	122.41	48.8
16H-2, 130–150	137.40	44.5
16H-5, 121–141	141.81	44.1
17H-2, 130–150	146.90	42.1
17H-5, 80–100	150.90	41.6
19H-2, 130–150	158.16	37.4
19H-4, 130–150	161.09	35.4
20H-2, 130–150	165.98	36.1
20H-5, 130–150	170.48	32.0
22H-2, 130–150	175.50	30.7
22H-4, 128–148	178.48	22.4
23H-2, 130–150	185.00	25.3
23H-4, 102–122	187.72	19.0
26X-2, 130–150	207.00	BDL
26X-4, 130–150	209.88	BDL
27X-5, 125–150	220.75	BDL
28X-4, 125–150	228.85	BDL
29X-2, 125–150	235.55	BDL
30X-4, 110–135	248.00	BDL
31X-2, 116–141	254.76	BDL
204-1252A-		
1H-1, 135–150	1.35	46.0
1H-2, 135–150	2.85	41.0
1H-3, 85–100	3.85	30.1
2H-6, 135–150	13.75	26.0
3H-5, 135–150	20.50	51.1
4H-5, 135–150	31.13	60.0
5H-2, 135–150	35.34	63.4
6H-5, 135–150	50.25	65.4
7H-5, 135–150	59.75	68.3
8H-2, 135–150	64.75	73.3
9H-2, 135–150	74.25	62.2
9H-5, 135–150	78.75	64.6
10H-2, 45–60	82.85	58.0
11H-2, 135–150	93.25	58.6
12H-2, 135–150	102.75	52.6
13H-2, 135–150	112.25	57.5
14H-2, 135–150	121.75	93.9*
15X-2, 135–150	127.85	42.4
15X-5, 130–150	132.18	32.8
16X-2, 130–150	137.50	29.3
16X-4, 130–150	140.50	14.3
17X-5, 120–140	151.60	14.3
18X-2, 130–150	156.90	14.3
20X-2, 130–150	176.30	13.6
21X-5, 130–150	190.36	13.2
24X-3, 130–150	215.50	11.3
26X-3, 130–150	234.80	9.8
28X-3, 130–150	254.14	BDL
201-1230A-		
2H-5, 135–150	12.15	35.6
4H-5, 135–150	31.15	48.1
5H-5, 135–150	40.65	61.2
6H-3, 143–158	47.23	52.1
6H-5, 135–150	50.23	46.7
8H-3, 135–150	58.65	37.8
9H-4, 125–140	65.35	33.3
10H-3, 135–150	74.65	26.4
11H-5, 135–150	87.15	28.4
12H-2, 135–150	92.15	21.6
13H-5, 135–150	106.15	13.4
14H-5, 135–150	115.72	BDL
15H-2, 135–150	119.47	29.0
17H-1, 135–150	130.65	34.0
17H-3, 135–150	133.65	19.5
18H-2, 135–150	141.65	28.2
19H-1, 135–150	149.65	25.0
21H-3, 135–150	161.63	23.6
24H-2, 0–98	188.80	28.6
26H-1, 82–97	199.62	19.9
33X-1, 130–150	235.70	16.6
38X-2, 0–19	268.70	16.6

Notes: BDL = below detection limit of 9 μM. * = value seems too high.